

Cold hybrid electrical-optical ion trap

Jin-Ming Cui,^{1,2,3,4,*} Shi-Jia Sun,^{5,3} Xi-Wang Luo,^{5,2,3,3,†} Yun-Feng Huang,^{5,2,3,4} Chuan-Feng Li,^{5,2,3,4,‡} and Guang-Can Guo^{5,2,3}

¹*Laboratory of Quantum Information, University of Science and Technology of China, Hefei 230026, China*

²*Anhui Province Key Laboratory of Quantum Network,*

University of Science and Technology of China, Hefei 230026, China

³*CAS Center for Excellence in Quantum Information and Quantum Physics,*

University of Science and Technology of China, Hefei 230026, China

⁴*Hefei National Laboratory, University of Science and Technology of China, Hefei 230088, China*

⁵*CAS Key Laboratory of Quantum Information, University of Science and Technology of China, Hefei 230026, China*

(Dated: June 4, 2025)

Advances in research such as quantum information and quantum chemistry require subtle methods for trapping particles (including ions, neutral atoms, molecules, etc.). Here we propose a hybrid ion trapping method by combining a Paul trap with optical tweezers. The trap combines the advances of the deep-potential feature for the Paul trap and the micromotion-free feature for the optical dipole trap. By modulating the optical-dipole trap synchronously with the radio frequency voltage of the Paul trap, the alternating electrical force in the trap center is fully counteracted, and the micromotion temperature of a cold trapped ion can reach the order of nK while the trap depth is beyond 300K. These features will enable cold collisions between an ion and an atom in the s -wave regime and stably trap the produced molecular ion in the cold hybrid system. This will provide a unique platform for probing the interactions between the ions and the surrounding neutral particles and enable the investigation of new reaction pathways and reaction products in the cold regime.

I. INTRODUCTION

Near absolute zero temperatures, cold chemistry unveils intricate quantum processes within reaction mechanisms, garnering significant attention across both chemical and physical disciplines [1–12]. In the last decade, an emerging area of cold hybrid ion-atom systems has been developed as a new platform for fundamental research, which is dedicated to controlling the cold collision and quantum chemistry of ions and atoms [13–19]. Binding the neutral atom and ion and then stably trapping the produced molecular ion are prerequisites for exploring the quantum features of the molecular ion. To investigate collision physics in the quantum regime of the cold hybrid ion-atom system, reaching the single partial wave limit (i.e., the s -wave limit) is an important step [14]. Although the trapped ion can be cooled close to the quantum collision regime using buffer atomic gases with a large ion-atom mass ratio [20], the micromotion of the Paul trap (PT) heats the system away from a stable bound state [21–23], which hinders progress in this area. Pioneering experiments using optical dipole traps (ODTs) to capture ions were demonstrated [24–27], which is a potential solution to the micromotion heating problem in the cold hybrid ion-atom system. However, because the dipole potential is shallow, it is quite challenging to keep the ion during the reaction and stably trap the produced molecular ion.

In this work, we propose a novel hybrid electrical-optical ion trap that combines the advantages of the deep-potential feature of a PT and the micromotion-free feature of an ODT. The key idea is to counteract the alternating electrical force around the center of a PT that is responsible for the micromotion problem, which is achieved by introducing optical-dipole traps that are modulated synchronously with the radio frequency (RF) voltage of the PT. This hybrid electrical-optical trap corresponds to a deep PT with a micromotion-free dip at the center, and this potential structure provides an ideal platform for studying low-energy physics (such as cold collisions and cold chemistry). Since the center dip provides a micromotion-free area for the trapped ion to interact with a neutral atom, the produced molecular ion can be stably kept in a deep background potential profile provided by the PT. To analyze the performance of the trap, we consider counteracting 99% of the alternating force which is experimentally reasonable. The intrinsic micromotion (iMM) energy can be suppressed by four orders of magnitude. Under current voltage compensation techniques in trapped ion fields [28], the DC stray field can be suppressed below 1 V/m, which leads to the ultimate cold ion excess micromotion (eMM) temperature in the hybrid trap below 1 nK. Under such cold ion temperatures, many ion-atom s -wave scattering processes can be investigated. Moreover, by simulating a cold collision process between a Yb^+ ion and a Rb atom, we find that the hybrid trap effectively solves the micromotion heating problem, which dissociates the ion-atom bound state in the cold collision process. The proposed hybrid trap offers a simple yet powerful platform to study ion-atom collisions in the quantum regime, which paves the way for exploring novel reactions and manipulating the produced

* jmcui@ustc.edu.cn

† luoxw@ustc.edu.cn

‡ cfli@ustc.edu.cn

molecular ion in such cold hybrid systems.

II. SCHEME AND RESULTS

Our scheme employs modulating optical tweezers to counteract the alternating force caused by the RF electrical field. If we consider a hybrid trap consisting of a PT and N modulating ODTs, the total potential of the trap is

$$U(\mathbf{r}, t) = U_E(\mathbf{r}) + \tilde{U}_E(\mathbf{r}) \cos(\Omega t) + \sum_i^N U_{D,i}(\mathbf{r}) [1 + \eta_i \cos(\Omega t)], \quad (1)$$

where $U_E(\mathbf{r})$ and $\tilde{U}_E(\mathbf{r})$ are the potentials generated by the DC field and RF field of the PT respectively, $U_{D,i}(\mathbf{r})$ is the potential of i 'th ODT, and η_i is the modulation depth of i 'th ODT with $|\eta_i| \leq 1$. When the ion is cooled to a low temperature (e.g., via Doppler cooling to several millikelvin), its motional range becomes significantly smaller than the characteristic size of the Paul trap and the optical dipole trap (ODT). Supposing the centers of all traps overlap each other for simplicity, the potentials around the trap center can be expanded as harmonic forms

$$U_E(\mathbf{r}) = k_0^x x^2 + k_0^y y^2 + k_0^z z^2 + C_E, \quad (2)$$

$$\tilde{U}_E(\mathbf{r}) = k_1^x x^2 + k_1^y y^2 + k_1^z z^2 + \tilde{C}_E, \quad (3)$$

$$U_{D,i}(\mathbf{r}) = K_i^x x^2 + K_i^y y^2 + K_i^z z^2 + C_{D,i}, \quad (4)$$

where C_E , \tilde{C}_E and $C_{D,i}$ are constants. $U_E(\mathbf{r})$ and $\tilde{U}_E(\mathbf{r})$ generated by electrical fields have to fulfill the Laplace equation $\Delta U(\mathbf{r}) = 0$, which leads to restrictions in the geometric factors,

$$k_0^x + k_0^y + k_0^z = 0, \quad (5)$$

$$k_1^x + k_1^y + k_1^z = 0, \quad (6)$$

while $U_{D,i}(\mathbf{r})$ is not restricted by this condition. The alternating force strength of the hybrid trap is $\tilde{\mathbf{F}}(\mathbf{r}) = \nabla(\tilde{U}_E + \sum \eta_i U_{D,i})$, so eliminating the force to zero leads to the condition

$$k_1^\gamma + \sum_i^N \eta_i K_i^\gamma = 0, \quad (7)$$

for all $\gamma \in \{x, y, z\}$, which can be achieved by setting the modulation depths and geometric shapes of ODTs.

Supposing we use astigmatic Gaussian spots to generate the dipole traps required. The intensity profile of a focused astigmatic Gaussian beam along axis c in coordinate $(\hat{a}, \hat{b}, \hat{c})$ can be written as

$$I(\mathbf{r}) = I_0 \frac{w_{0a}}{w_a(c)} \frac{w_{0b}}{w_b(c)} \exp \left\{ -2 \left[\frac{a^2}{w_a(c)^2} + \frac{b^2}{w_b(c)^2} \right] \right\}, \quad (8)$$

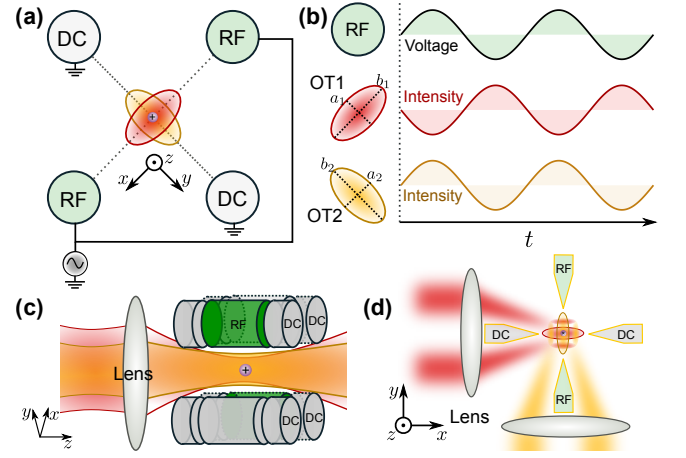


FIG. 1. Scheme of a hybrid electrical-optical ion trap. (a) The trap consists of a Paul trap (e.g., a four-rod trap or a blade trap) and two modulating optical dipole traps (ODTs) with different oriented astigmatic spots. (b) The phase relation between the RF voltage of the Paul trap and the optical intensities of the two ODTs. (c, d) two feasible realizations of the hybrid trap.

where $w_{a/b}(c) = w_{0,a/b} \sqrt{1 + (c/z_{Ra/b})^2}$ are the beam waists for a and b axes, i.e., short and long axes respectively, $z_{Ra/b} = \pi w_{0,a/b}^2 / \lambda$ are the Rayleigh ranges and λ is the wavelength. As the potential of ODT is proportional its intensity $U_{D,i}(\mathbf{r}) \propto I_{D,i}(\mathbf{r})$, by expanding it near the zero point, the potential coefficients are

$$K_i^a = \frac{2U_{0i}}{w_{0,ai}^2}, K_i^b = \frac{2U_{0i}}{w_{0,bi}^2}, \quad K_i^c = \frac{U_{0i}\lambda^2}{2\pi^2} \left(\frac{1}{w_{0,ai}^4} + \frac{1}{w_{0,bi}^4} \right), \quad (9)$$

where $U_{0i} = \frac{\pi c^2 \Gamma}{2\omega_0^3} \left(\frac{2}{\Delta_2} + \frac{1}{\Delta_1} \right) I_{0i}$ [29]. Finding a proper set of $\{\eta_i U_{0i}, w_{0,ai}, w_{0,bi}\}$ to satisfy Eq. 7 and Eq. 9 will eliminate the alternation force at the trap center.

Figure 1(c,d) shows two feasible configurations to demonstrate the scheme in a symmetric linear PT with four rods or blades [30, 31]. For simplicity, we take Fig. 1(c) for example, where two optical tweezers with focused astigmatic Gaussian spots are applied on the trapped ion with similar beam waists, i. e., $w_{0,a1} = w_{0,a2} = w_a$, $w_{0,b1} = w_{0,b2} = w_b$, $U_{01} = U_{02} = U_0$, and the long axes of two two ODTs are perpendicular to each other, i.e. $\hat{a}_1 \perp \hat{a}_2 \parallel \hat{y}$, $\hat{b}_1 \perp \hat{b}_2 \parallel \hat{x}$. The symmetric linear PT condition requires $k_1^x = -k_1^y = k_1$, $k_1^z = 0$. Suppose $\eta_1 = -\eta_2 = 1$, which indicates modulations between two ODTs have a π phase difference (shown in Fig. 1(b)), then the configurations of the ODTs can be

$$\begin{aligned} k_1 &= k_a - k_b, \\ K_1^x &= K_2^y = k_a, \\ K_1^y &= K_2^x = k_b, \end{aligned} \quad (10)$$

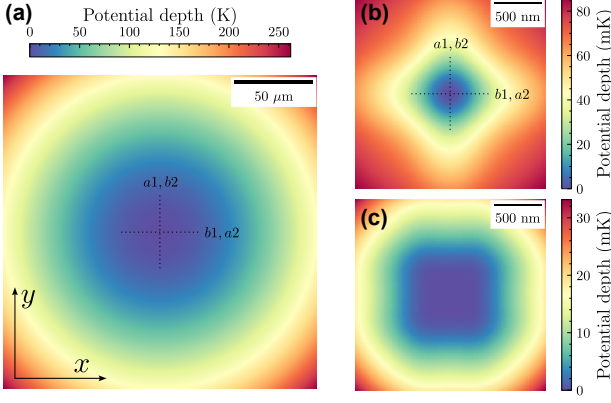


FIG. 2. Pseudo potential of a hybrid trap for $^{171}\text{Yb}^+$. (a) The total pseudo potential of the trap, indicating a deep potential. (b,c) The constant part and the alternating part of the pseudo potential near the trap center, respectively. The alternating pseudo potential is flat near the center, which indicates the alternating force is zero. The simulation condition is $\Omega = 2\pi \times 2$ MHz, $V_{RF} = 10$ V, $\kappa = 0.6$, $V_{DC} = 1$ V, $R = 0.5$ mm, $Z_0 = 1$ mm, $\omega_x = \omega_y = 2\pi \times 180$ kHz, $\omega_z = 2\pi \times 131$ kHz for the Paul trap, laser wavelength at 554.6 nm, $w_a = w_b/3 = 478$ nm can be generated through an objective with a numerical aperture (NA) of 0.6, $U_0/h = -622$ MHz for optical dipole traps.

where $k_{a,b} = 2U_0/w_{a,b}^2$.

The pseudo potential of the hybrid trap can be decomposed into a direct potential (DP) and an alternating potential (AP)

$$\Psi(\mathbf{r}) = \Phi_0(\mathbf{r}) + \frac{1}{4m\Omega^2} \|\nabla\Phi_1(\mathbf{r})\|^2, \quad (11)$$

where $\Phi_0(\mathbf{r}) = U_E(\mathbf{r}) + \sum_i^N U_{D,i}(\mathbf{r})$ and $\Phi_1(\mathbf{r}) = \tilde{U}_E(\mathbf{r}) + \sum_i^N \eta_i U_{D,i}(\mathbf{r})$ are the direct and alternating potentials respectively. For a symmetric linear PT [30], $k_0^x = k_0^y = -2k_0^z = -2\kappa QV_{DC}/Z_0^2$, $k_1^x = -k_1^y = QV_{RF}/2R^2$, $k_1^z = 0$, where κ is a geometric factor of the trap, Q is the charge of the ion, V_{DC} and V_{RF} are the DC and RF voltages applied to the trap, R is the perpendicular distance from the trap axis to the trap electrodes, Z_0 is the distance from the trap center to the endcap electrodes. The pseudo potential can be calculated by substituting Eq. 8-10 into Eq. 11. When the alternating force caused by the RF electrical field is completely compensated by the modulating ODTs, which we call the zero alternating trapping condition (ZATC), we can derive $U_0 = QV_{RF}w_a^2w_b^2/4R^2(w_a^2 - w_b^2)$. To make the condition realistic, a low RF voltage of PT and small spots of ODTs should be used to minimize the optical power of the ODT. Consequently, a lower RF frequency Ω is preferred to make a deeper pseudo potential under the low RF voltage. A numerical simulation result is shown in Fig. 2. In a large range, it acts as a PT with deep potential as Fig. 2(a). At the center of the trap, it acts as a tight ODT as Fig. 2(b). The alternating pseudo potential in Fig. 2(c) is flat, which indicates the alternating

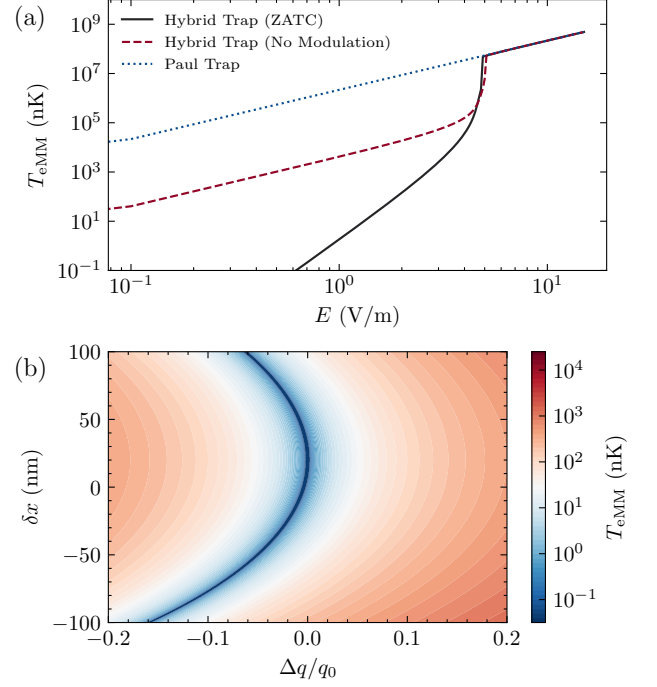


FIG. 3. Ion motion simulation for trapping temperature in a stray electrical field (SEF). (a) Excess micromotion (eMM) temperature of a trapped ion along with different SEFs. The hybrid trap provides a lower temperature than a PT under the same SEF. When the hybrid trap works at zero alternating trapping condition (ZATC), the ion's eMM temperature reaches nK under a SEF of 1 V/m. The direction of the SEF for simulation is (1,1,1). (b) Ion's eMM temperature simulation under experimental imperfections, δx : misalignment between Paul trap and the ODT, Δq : uncompensated alternating force factor. Intrinsic micromotion (iMM) is also suppressed, as the iMM temperature is scale as Δq^2 . The figure is calculated under a SEF of 1 V/m along the x axis. Hybrid trap and Paul trap parameters are the same as those in Fig. 2.

force is zero. With the simulation result, the required laser power is 0.7 W at 554.6 nm, if we use an objective with NA=0.6 to generate the required ODTs.

Next, we will discuss the cold trapped ion temperature limit in the hybrid trap. Supposing the ion oscillates near \mathbf{u}_0 in the hybrid trap under a stray electrical field \mathbf{E} , and has been cooled to a low temperature $|\mathbf{u} - \mathbf{u}_0| \ll w_a$, then the motion equation can be approximated as a Mathieu equation near \mathbf{u}_0

$$\ddot{u}_l + [a_l(\mathbf{u}_0) + 2q_l(\mathbf{u}_0) \cos(\Omega t)] \frac{\Omega^2}{4} u_l = \frac{Q \cdot E_l}{m}, \quad (12)$$

where $a_l(\mathbf{u}) = 4\hat{e}_l \cdot \nabla\Phi_0(\mathbf{u})/m\Omega^2 u_l$ and $q_l(\mathbf{u}) = 2\hat{e}_l \cdot \nabla\Phi_1(\mathbf{u})/m\Omega^2 u_l$. The equilibrium position \mathbf{u}_0 can be numerically solved by iterating

$$u_{0,l} = \frac{4Q \cdot E_l}{m\Omega^2 [a_l(\mathbf{u}) + q_l^2(\mathbf{u})/2]}. \quad (13)$$

TABLE I. ODT laser wavelengths for hybrid ion traps in different ion-atom systems. E_k is a characteristic energy scale of the ion-atom interaction [14], which is associated with the s -wave scattering limit. The wavelengths are chosen to ensure that the alternating ODT at a magic wavelength for the atom, minimizing the AC Stark shift of the atomic ground state. This prevents the ODT from driving the atom into micromotion as it approaches the ion.

Ion	Atom	λ_{ODT} (nm)	P (W)	E_k/k_B (nK)
Yb^+	Rb	420.6	0.24	44.7
Yb^+	Rb	422.3	0.25	44.7
Yb^+	Rb	787.4	1.48	44.7
Yb^+	Yb	554.63	0.70	44.7
Ca^+	Na	589.46	0.48	1370.7
Ca^+	Li	670.97	1.09	10601.5
Sr^+	Rb	787.41	0.94	77.8

The final temperature caused by excess micromotion is

$$T_{\text{eMM}} = \frac{m\Omega^2}{16k_B} \sum_l q_l^2(\mathbf{u}_0) u_{0,l}^2. \quad (14)$$

Using the above numerical method, we can study the ion eMM temperature under a large electrical field. Fig. 3(a) shows the comparison of trapped ion eMM temperature in three different traps under a stray electrical field along the (1,1,1) direction. The stray field will shift the trap center of the PT part of the hybrid trap while the ODT is not affected, so the total pseudo potential is a double well under a small stray field. The ion stays in the tight ODT under a small stray field, and the ion's eMM temperature will be low even without modulating the ODTs. By increasing the stray field, the ion will eventually be pushed from the ODT to PT, so the ion's eMM temperature of the hybrid trap is close to that of the PT, when the stray field is larger than 5 V/m.

In order to further insight the ion eMM temperature relation with experiment parameters (e. g., misalignment between PT and the ODT δx , stray electrical field E , residual alternating force (RAF) parameter $\Delta q = 4(k_1 + k_a - k_b)/m\Omega^2$), we study one dimensional motion for simplification. Considering the condition of small misaligned distance $\delta x \ll w_0$, the approximated ion eMM temperature can be derived as (see Appendix B)

$$T_{\text{eMM}} \approx \frac{m\Omega^2}{16k_B} \left(\Delta q + \frac{(\delta x - x_0)^2}{x_b^2} \right)^2 x_0^2, \quad (15)$$

where $x_0 \approx -Q \cdot E/(k_0 + 2k_a + 2k_b)$ is the ion position offset pushed by the stray electrical field, and $x_b^2 = m\Omega^2/8(k_b/w_b^2 - k_a/w_a^2)$. Fig. 3(b) demonstrates that the ion eMM temperature can reach the 100 nK level, even with a misalignment of approximately 50 nm and a RAF ratio of $\Delta q/q_0 = 5\%$ (where $q_0 = 4k_1/m\Omega^2$ is the q -factor of the bare Paul trap), under a stray field of

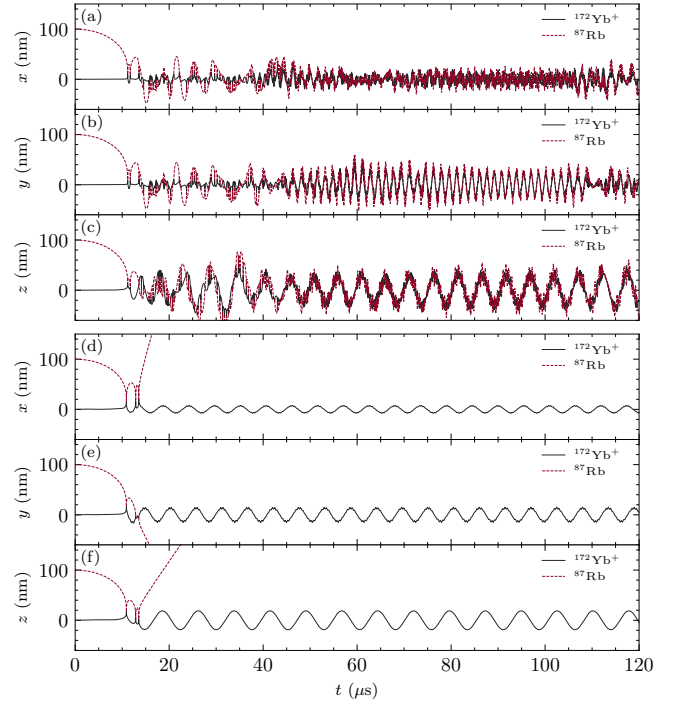


FIG. 4. Numerical simulations of a ion-atom (Rb and Yb^+) collision in a hybrid trap (a-c) and a bare Paul trap (d-f). For comparison, the hybrid trap has the same electric fields with configurations as Fig. 2. Rb approaching an Yb^+ initially stationed in trap center, the first hard-core collision time is at $t = 0$. In Paul trap, the ion is heated by the RF field and bounces out quickly, whereas in hybrid trap, the ion-atom can be weakly bounded. The harmonic frequencies of two traps are $\omega_{\text{Hybrid}} = 2\pi \times 0.84$ MHz and $\omega_{\text{Paul}} = 2\pi \times 0.18$ MHz, leading to the corresponding characteristic lengths $R_{\text{Hybrid}} = 33.4$ nm and $R_{\text{Paul}} = 55.9$ nm, respectively. The simulation method is modified from Ref. 21.

1 V/m along the x -axis. Single-particle localization microscopy has demonstrated sub-10 nm positioning accuracy in ion imaging systems [32–34]. By implementing a dual-objective configuration on a high-optical-access ion trap [35]—where opposing objectives are utilized with one generating optical tweezers and the other simultaneously imaging both ions and tweezer spots—we can achieve co-localization accuracy of less than 50 nm. This approach not only significantly reduces alignment complexity but also relaxes the trap alignment requirements in our scheme. Additionally, the ion iMM temperature and energy, which scale as Δq^2 (see Appendix B), can be reduced by four orders of magnitude with a 1% RAF ratio. The iMM temperature for the motional ground state of the bare Paul trap, calculated using the parameters in Fig. 2, is 2.73 μK . In contrast, for the hybrid trap with a RAF ratio of 1%, it is significantly reduced to 58.3 pK.

Finally, we will investigate the collision process between an ion and an atom in the hybrid trap. For this study, the laser wavelength of the ODT must be carefully selected based on the specific ion-atom pair. The alter-

nating ODT for the trapped ion should not contribute to the trapping potential for the atom. This requires the ODT wavelength to be chosen such that it does not create a trapping potential for the atom, ensuring that the AC Stark shift of the atomic ground state is minimized. If this condition is not met, the alternating ODT would drive the atom into micromotion as it approaches the ion, resulting in unwanted dynamics. The wavelengths listed in Tab. I are carefully chosen to satisfy this requirement while balancing the tradeoff between ODT power and detuning from atomic and ionic resonances. Tab. I lists several laser wavelengths for some composition of ion-atom species, and the laser power with hybrid trap setting as Fig. 2. We take Rb and Yb^+ in this investigation following the method presented in Ref. [21], with details in Appendix C. When an ion moves in a PT without any disturbance, the RF field does zero work on the ion for an RF period. However, in the cold hybrid ion-atom system, the polarized atom will exert an attraction force on the ion (by attraction potential $V(r) = -C_4/r^4$) and thus disturb the conserved cycle of energy transfer, and finally the ion-atom system gains net energy from the RF field, which increases the temperature of the system. A characteristic length scale $R = \sqrt[6]{2C_4/m_i\omega^2}$ is preferred to be used (when the interaction potential $V(r)$ is equal in magnitude to the trap harmonic potential, where $\omega = \Omega\sqrt{a + q^2/2}/2$ is the secular frequency of the ion near the trap center). In a PT (Fig. 4(b)), the ion gains enough energy from the RF field when the atom approaches, and after one collision, the atom escapes. In the hybrid trap (Fig. 4(a)), since the alternating force induced by the RF field near the trap center is compensated, the ion-atom system nearly undergoes an energy-conservative process and forms a weakly bound ion-atom pair, keeping a low temperature. In the hybrid trap, the corresponding characteristic energy scale is no longer restricted by the RF heating but determined by the atomic gas temperature, which enables access to the regimes of the s -wave limit or quantized ion motion in the cold hybrid system. The work done by the RAF during a collision depends on the phase ϕ at the time of the close-range collision, which can be written as (see Appendix D)

$$W = \frac{1}{2}\mu\Omega^2 R^2 \sin\phi \cdot \left(\Delta q\eta_1 + \frac{R^4}{r_0^2 x_b^2} \eta_2 \right)$$

where $\mu = m_i m_a / (m_i + m_a)$ is the reduced mass, $\eta_1 = 2/3 \int_0^{\Omega t_1} (A - B\tau^{1/3}) \cdot \tau^{-2/3} \sin\tau \cdot d\tau$ and $\eta_2 = 2/3 \int_0^{\Omega t_1} (A - B\tau^{1/3})^3 \cdot \tau^{-2/3} \sin\tau \cdot d\tau$ are integrals with parameters $A = r_c r_0 / R^2$, $B = \mu r_0^2 / m_i R^2$, the ion's displacement from the trap center r_c for the collision position and a characteristic length $r_0 = \sqrt[6]{18C/\mu\Omega^2}$. Fig. 4(a) shows r_c is distributed in $0 \sim 20$ nm for multi hard-core collisions, indicating that the max work done by RAF for one collision is on the order of tens of nK $\cdot k_B$.

Conclusion and discussion.— In summary, we proposed a novel hybrid trap consisting of a PT and modulated ODTs that takes advantage of the deep-potential

feature of the PT while eliminating the micromotion problem in the cold hybrid ion-atom system. The trap can suppress the micromotion temperature to the order of nK, offering a new route to reach the quantum collision in the ion-atom mixture. Our proposed schemes are quite feasible since an ion trap system with high optical accessibility has been demonstrated in [35]. Compared with previous optical trapping methods for ions where the PT is switched off [24–27], our scheme can stably trap elementary and molecular ions all through the cold ion-atom collision process due to the always-on PT, which provides an ideal platform for studying cold ion-atom collision and reaction and investigating the properties of the produced molecular ion.

ACKNOWLEDGMENTS

This work was supported by the National Key Research and Development Program of China (No. 2017YFA0304100, 2024YFA1409403), the National Natural Science Foundation of China (Grant No. 11774335, No. 11734015, and No. 12204455), the Key Research Program of Frontier Sciences, CAS (Grant No. QYZDY-SSWSLH003), and the Innovation Program for Quantum Science and Technology (Grant No. 2021ZD0301604 and No. 2021ZD0301200).

J.-M. Cui and S.-J. Sun contributed equally to this work. Innovation Program for Quantum Science and Technology

The data that support the findings of this article are openly available [36]

Appendix A: Ion Dynamics in the Hybrid Trap Potential

The electrical potential of a classical Paul trap is

$$U_{\text{Paul}}(\mathbf{r}, t) = U_E(\mathbf{r}) + \tilde{U}_E(\mathbf{r}) \cos(\Omega t), \quad (\text{A1})$$

where $U_E(\mathbf{r})$ and $\tilde{U}_E(\mathbf{r})$ are the potentials generated by the DC and RF fields respectively. For a symmetric linear Paul trap with four rods or blades, the electrical potentials can be expressed as [30]

$$U_E(\mathbf{r}) = k_0 z^2 - \frac{1}{2} k_0 (x^2 + y^2), \quad (\text{A2})$$

$$\tilde{U}_E(\mathbf{r}) = k_1 (x^2 - y^2) + V_{RF}/2, \quad (\text{A3})$$

where $k_0 = \kappa Q V_{DC} / Z_0^2$, $k_1 = Q V_{RF} / 2R^2$, where κ is a geometric factor of the trap, Q is the charge of the ion, V_{DC} and V_{RF} are the DC and RF voltages applied on the trap, R is the perpendicular distance from the trap axis to the trap electrodes, Z_0 is the distance from the trap center to the end-cap electrodes. The equations of motion for a single ion of mass m in the above potential

are give by Mathieu equations

$$\ddot{u}_l + [a_{0,l} + 2q_{0,l} \cos(\Omega t)] \frac{\Omega^2}{4} u_l = 0, \quad (\text{A4})$$

where $\mathbf{u} = u_x \hat{x} + u_y \hat{y} + u_z \hat{z}$ is the position of the ion and

$$a_{0,x} = a_{0,y} = -\frac{1}{2}a_{0,z} = a_0 = \frac{4k_0}{m\Omega^2}, \quad (\text{A5})$$

$$q_{0,x} = -q_{0,y} = q_0 = \frac{4k_1}{m\Omega^2}, \quad (\text{A6})$$

$$q_{0,z} = 0. \quad (\text{A7})$$

The potential generated by the hybrid trap is,

$$U(\mathbf{r}, t) = U_E(\mathbf{r}) + \tilde{U}_E(\mathbf{r}) \cos(\Omega t) + \sum_{i=1} U_{D,i}(\mathbf{r}) [1 + \eta_i \cos(\Omega t)], \quad (\text{A8})$$

$$= \Phi_0(\mathbf{r}) + \Phi_1(\mathbf{r}) \cos(\Omega t) \quad (\text{A9})$$

where $U_{D,i}(\mathbf{r})$ is the potential of i 'th ODT, η_i is the modulation depth of the ODT, $\Phi_0(\mathbf{r}) = U_E(\mathbf{r}) + \sum_i^N U_{D,i}(\mathbf{r})$ and $\Phi_1(\mathbf{r}) = \tilde{U}_E(\mathbf{r}) + \sum_i^N \eta_i U_{D,i}(\mathbf{r})$ are the direct and alternating potentials respectively. If we use the two dipole trap scheme in the main text and use the zero alternating trapping condition, the modulation parameters will be $\eta_1 = -\eta_2 = 1$. The potential of ODTs are [29]

$$U_D(\mathbf{r}) = \frac{\pi c^2 \Gamma}{2\omega_0^3} \left(\frac{2}{\Delta_2} + \frac{1}{\Delta_1} \right) I(\mathbf{r}), \quad (\text{A10})$$

where $I(\mathbf{r})$ is the intensity of the specified ODT, Γ is the damping rate of P state, Δ_2 is the laser detuning

from $S_{1/2}$ to $P_{3/2}$ transition, Δ_1 is the laser detuning from $S_{1/2}$ to $P_{1/2}$ transition, and ω_0 is the ODT laser frequency. The intensity profile of a focused astigmatic Gaussian beam along axis \hat{c} in coordinate $(\hat{a}, \hat{b}, \hat{c})$ can be written as

$$I(\mathbf{r}) = I_0 \frac{w_{0a}}{w_a(c)} \frac{w_{0b}}{w_b(c)} \exp \left\{ -2 \left[\frac{a^2}{w_a(c)^2} + \frac{b^2}{w_b(c)^2} \right] \right\}, \quad (\text{A11})$$

where $w_{a/b}(c) = w_{0,a/b} \sqrt{1 + (c/z_{Ra/b})^2}$ are the beam waists for a and b axes, i. e. short and long axes respectively, $z_{Ra/b} = \pi w_{0,a/b}^2 / \lambda$ are the Rayleigh ranges and λ is the ODT laser wavelength. Applying the scheme with two orthogonal astigmatic Gaussian beam spots at $z = 0$ in the main text, the potentials are

$$\Phi_0(x, y, 0) = k_0 z^2 - \frac{1}{2} k_0 (x^2 + y^2) + U_0 \exp(-2x^2/w_a^2 - 2y^2/w_b^2) + U_0 \exp(-2x^2/w_b^2 - 2y^2/w_a^2), \quad (\text{A12})$$

$$\Phi_1(x, y, 0) = k_1 (x^2 - y^2) + U_0 \exp(-2x^2/w_a^2 - 2y^2/w_b^2) - U_0 \exp(-2x^2/w_b^2 - 2y^2/w_a^2), \quad (\text{A13})$$

where $U_0 = \pi c^2 \Gamma (\Delta_2 + 2\Delta_1) I_0 / 2\omega_0^2 \Delta_2 \Delta_1$. Expanding $\Phi_1(x, y, 0)$ near the trap center ($x = 0, y = 0$) and setting the alternating force $\nabla \Phi_1$ to zero, we can derive the zero alternating potential condition (ZATC)

$$U_{0,\text{ZACT}} = \frac{k_1 w_a^2 w_b^2}{2(w_a^2 - w_b^2)}. \quad (\text{A14})$$

For the other arbitrary U_0 , there will be residual alternating forces (RAFTs) near the trap center, in this case, we can define a RAF parameter $\Delta q = 4(k_1 + k_a - k_b)/m\Omega^2$ (where $k_{a,b} = 2U_0/w_{a,b}^2$, see the subsection B 2). Comparing the original Paul trap, a ratio of RAF of the hybrid trap can be defined as $\beta = \Delta q/q_0$.

To study three-dimensional dynamics of a single ion in the hybrid trap, we can perform numerical simulation

by reserving the full form of the potentials. We take the equation along the x axis for example. From the equation of motion driven by forces

$$m\ddot{x} = -\frac{\partial U(\mathbf{r}, t)}{\partial x} = -\frac{\partial \Phi_0}{\partial x} - \frac{\partial \Phi_1}{\partial x} \cos(\Omega t), \quad (\text{A15})$$

we can get

$$\ddot{x} + [a_x(x, y, z) + 2q_x(x, y, z) \cos(\Omega t)] \frac{\Omega^2}{4} x = 0, \quad (\text{A16})$$

where

$$a_x(x, y, z) = \frac{4}{m\Omega^2} \frac{\partial \Phi_0}{x \partial x},$$

$$q_x(x, y, z) = \frac{2}{m\Omega^2} \frac{\partial \Phi_1}{x \partial x},$$

are Mathieu equation parameters that depend on the

ion's position. The position dependent Mathieu equation parameters in three dimensions can be deduced as

$$\begin{aligned} a_x(x, y, z) &= \frac{4}{m\Omega^2} \left[-k_0 - U_0 g(z) \left(f_1(x, y, z) \frac{4}{w_a^2(z)} + f_2(x, y, z) \frac{4}{w_b^2(z)} \right) \right], \\ a_y(x, y, z) &= \frac{4}{m\Omega^2} \left[-k_0 - U_0 g(z) \left(f_1(x, y, z) \frac{4}{w_b^2(z)} + f_2(x, y, z) \frac{4}{w_a^2(z)} \right) \right], \\ a_z(x, y, z) &= \frac{4}{m\Omega^2} [2k_0 + U_0 g(z) (f_1 M_1 + f_2 M_2) + U_0 N(z) (f_1 + f_2)], \end{aligned} \quad (\text{A17})$$

and

$$\begin{aligned} q_x(x, y, z) &= \frac{2}{m\Omega^2} \left[2k_1 + U_0 g(z) \left(f_1(x, y, z) \frac{4}{w_a^2(z)} - f_2(x, y, z) \frac{4}{w_b^2(z)} \right) \right], \\ q_y(x, y, z) &= \frac{2}{m\Omega^2} \left[-2k_1 + U_0 g(z) \left(f_1(x, y, z) \frac{4}{w_b^2(z)} - f_2(x, y, z) \frac{4}{w_a^2(z)} \right) \right], \\ q_z(x, y, z) &= \frac{2}{m\Omega^2} [U_0 g(z) (f_1 M_1 - f_2 M_2) + U_0 N(z) (f_1 - f_2)], \end{aligned} \quad (\text{A18})$$

where

$$f_1(x, y, z) = \exp[-2x^2/w_a^2(z) - 2y^2/w_b^2(z)] \quad (\text{A19})$$

$$f_2(x, y, z) = \exp[-2x^2/w_b^2(z) - 2y^2/w_a^2(z)] \quad (\text{A20})$$

$$g(z) = \frac{1}{\sqrt{1 + (z/z_{Ra})^2} \sqrt{1 + (z/z_{Rb})^2}} \quad (\text{A21})$$

$$N(z) = -g(z) \left(\frac{1}{z_{Ra}^2 + z^2} + \frac{1}{z_{Rb}^2 + z^2} \right) \quad (\text{A22})$$

$$M_1(x, y, z) = \frac{4x^2}{w_{0,a}^2 z_{Ra}^2 \alpha_a^4(z)} + \frac{4y^2}{w_{0,b}^2 z_{Rb}^2 \alpha_b^4(z)} \quad (\text{A23})$$

$$M_2(x, y, z) = \frac{4x^2}{w_{0,b}^2 z_{Rb}^2 \alpha_b^4(z)} + \frac{4y^2}{w_{0,a}^2 z_{Ra}^2 \alpha_a^4(z)} \quad (\text{A24})$$

and $w_{a/b}^2(z) = w_{0,a/b}^2 \alpha_{a/b}^2(z)$, $\alpha_{a/b}(z) = \sqrt{1 + (z/z_{Ra/b})^2}$, $z_{Ra/b} = \pi w_{0,a/b}^2 / \lambda$.

In the presence of a stray electrical field $\mathbf{E} = E_x \hat{x} + E_y \hat{y} + E_z \hat{z}$, the equations of motion will be

$$\ddot{x} + [a_x(x, y, z) + 2q_x(x, y, z) \cos(\Omega t)] \frac{\Omega^2}{4} x = \frac{Q \cdot E_x}{m}, \quad (\text{A25})$$

$$\ddot{y} + [a_y(x, y, z) + 2q_y(x, y, z) \cos(\Omega t)] \frac{\Omega^2}{4} y = \frac{Q \cdot E_y}{m}, \quad (\text{A26})$$

$$\ddot{z} + [a_z(x, y, z) + 2q_z(x, y, z) \cos(\Omega t)] \frac{\Omega^2}{4} z = \frac{Q \cdot E_z}{m}. \quad (\text{A27})$$

TABLE II. Numerical simulation parameters for trapping $^{171}\text{Yb}^+$. The shared trap parameters with $\Omega = 2\pi \times 2$ MHz (RF frequency), $\kappa = 0.6$, $V_{DC} = 1$ V, $V_{RF} = 10$ V, $R = 0.5$ mm and $Z_0 = 1$ mm.

	Paul Trap	Hybrid Trap
a_x	-8.575×10^{-3}	
a_y	-8.575×10^{-3}	
a_z	17.15×10^{-3}	
q_x	0.286	
q_y	-0.286	
q_z	0	
$\omega_x/2\pi$	179.7 kHz	840.2 kHz
$\omega_y/2\pi$	179.7 kHz	840.2 kHz
$\omega_z/2\pi$	131.0 kHz	131.0 kHz

Appendix B: Ion Micromotion temperature

1. Micromotion temperature of a trapped ion

The Mathieu equation when DC field \mathbf{E} shifts the equilibrium position of the ion writes Berkeland *et al.* [30]

$$\ddot{u}_l + [a_l + 2q_l \cos(\Omega t)] \frac{\Omega^2}{4} u_l = \frac{Q \cdot E_l}{m},$$

and the solution is

$$u_l(t) = (u_{0,l} + u_{1,l} \cos(\omega_l t + \varphi_l)) \left(1 + \frac{q_l}{2} \cos(\Omega t) \right),$$

where the equilibrium position

$$u_{0,l} \cong \frac{4Q \cdot E_l}{m\Omega^2(a_l + q_l^2/2)}, \quad (\text{B1})$$

and $u_{1,l}$ is the secular motion amplitude. The average kinetic energy due to motion along \hat{u}_l is

$$\begin{aligned} E_{k,l} &= \frac{1}{4} m u_{1,l}^2 (\omega_l^2 + \frac{1}{8} q_l^2 \Omega^2) + \frac{m \Omega^2}{16} q_l^2 u_{0,l}^2, \\ &= \frac{1}{4} m u_{1,l}^2 \omega_l^2 + \frac{1}{32} m q_l^2 u_{1,l}^2 \Omega^2 + \frac{m \Omega^2}{16} q_l^2 u_{0,l}^2 \\ &= E_{0,l} + E_{\text{iMM},l} + E_{\text{eMM},l} \end{aligned} \quad (\text{B2})$$

where the second and third term represent the kinetic energy due to intrinsic micromotion (iMM) and excess micromotion (eMM) along \hat{u}_l , respectively. So the temperature caused by the eMM in all directions reads

$$T_{\text{eMM}} = \sum_l \frac{E_{\text{eMM},l}}{k_B} = \frac{m \Omega^2}{16 k_B} \sum_l q_l^2 u_{0,l}^2. \quad (\text{B3})$$

T_{eMM} represents the lowest attainable temperature caused by excess micromotion of an ion in the trap, it can be zero in theory by setting $u_{0,l} = 0$, however experimental technics on adjusting the voltages on DC electrodes limit achievable T_{eMM} . The temperature caused by the iMM is

$$T_{\text{iMM}} = \sum_l \frac{E_{\text{iMM},l}}{k_B} = \frac{m \Omega^2}{32 k_B} \sum_l q_l^2 u_{1,l}^2. \quad (\text{B4})$$

Even in the condition that the secular motion is cooled to its ground state (when $u_{1,l} = \sqrt{\hbar/2m\omega_l}$) and the eMM is well compensated, the ion still has a temperature limit caused by the iMM

$$T_{0,\text{iMM}} = \frac{\hbar \Omega^2}{64 k_B} \sum_l \frac{q_l^2}{\omega_l}. \quad (\text{B5})$$

With trap parameters in Tab. II, the $T_{0,\text{iMM}}$ of the Paul trap is 2.73 μK . Considering a ratio of RAF $\beta = \Delta q/q_0 = 1\%$ for a hybrid trap, which is achievable in experiment, the corresponding $T_{0,\text{iMM}}$ is 58.3 pK.

Now we consider the case that the Mathieu equation parameters are in a position-dependent form: $a_l(\mathbf{u})$, $q_l(\mathbf{u})$. If the ion oscillates near \mathbf{u}_0 in the hybrid trap under a stray electrical field \mathbf{E} , and it has been cooled to a low temperature $|\mathbf{u} - \mathbf{u}_0| \ll w_a$, then the Mathieu equation can be approximated as

$$\ddot{u}_l + [a_l(\mathbf{u}_0) + 2q_l(\mathbf{u}_0) \cos(\Omega t)] \frac{\Omega^2}{4} u_l = \frac{Q \cdot E_l}{m}, \quad (\text{B6})$$

where the equilibrium position \mathbf{u}_0 can be numerically solved by iterating

$$u_{0,l}^{i+1} = \frac{4Q \cdot E_l}{m \Omega^2 [a_l(\mathbf{u}_0^i) + q_l^2(\mathbf{u}_0^i)/2]},$$

with an initial position $\mathbf{u}_0^0 = (0, 0, 0)$. Once the equilibrium position \mathbf{u}_0 is solved, we can get the temperature caused by excess micromotion

$$T_{\text{eMM}} = \frac{m \Omega^2}{16 k_B} \sum_l q_l^2(\mathbf{u}_0) u_{0,l}^2. \quad (\text{B7})$$

2. Approximated ion's eMM temperature expression

Take Paul trap center as the origin of coordinate, supposing we use full modulation, and the misalignment between the Paul trap and the ODT is δx . We define $\Delta x = x - \delta x$, then we can get the approximation at $(x, 0, 0)$

$$\begin{aligned} a_x(x) &= \frac{4}{m \Omega^2} \left[-k_0 - U_0 \left(e^{-2\Delta x^2/w_a^2} \frac{4}{w_a^2} + e^{-2\Delta x^2/w_b^2} \frac{4}{w_b^2} \right) \right] \\ &\approx -\frac{4}{m \Omega^2} [k_0 + 2k_a + 2k_b - 4(k_a/w_a^2 + k_b/w_b^2) \Delta x^2] \\ &= a - (x - \delta x)^2/x_a^2, \end{aligned} \quad (\text{B8})$$

$$\begin{aligned} q_x(x) &= \frac{2}{m \Omega^2} \left[2k_1 + U_0 \left(e^{-2\Delta x^2/w_a^2} \frac{4}{w_a^2} - e^{-2\Delta x^2/w_b^2} \frac{4}{w_b^2} \right) \right] \\ &\approx \frac{4}{m \Omega^2} [k_1 + (k_a - k_b) + 2(k_b/w_b^2 - k_a/w_a^2) \Delta x^2] \\ &= \Delta q + (x - \delta x)^2/x_b^2, \end{aligned} \quad (\text{B9})$$

where $k_{a,b} = 2U_0/w_{a,b}^2$, $a = -4(k_0 + 2k_a + 2k_b)/m\Omega^2$, $\Delta q = 4(k_1 + k_a - k_b)/m\Omega^2$, $x_a^2 = -m\Omega^2/16(k_a/w_a^2 + k_b/w_b^2)$ and $x_b^2 = m\Omega^2/8(k_b/w_b^2 - k_a/w_a^2)$. The trap center will shift to an equilibrium position under a stray field \mathbf{E}

$$x_0 = \frac{4Q \cdot E}{m \Omega^2 (a + \Delta q^2/2)} \approx \frac{4Q \cdot E}{m \Omega^2 a} = -\frac{Q \cdot E}{k_0 + 2k_a + 2k_b}.$$

Combined with Eq. B3, the approximated eMM temperature expression in this situation reads

$$\begin{aligned} T_{\text{eMM}} &\approx \frac{m \Omega^2}{16 k_B} q_x^2(x_0, 0, 0) x_0^2 \\ &\approx \frac{m \Omega^2}{16 k_B} \left(\Delta q + \frac{(x_0 - \delta x)^2}{x_b^2} \right)^2 x_0^2, \end{aligned}$$

which clearly illustrates the roles that imperfections Δq , δx play in restricting the lowest attainable temperature. In this expression, we approximate the iterated equilibrium position u_0 to x_0 , which represents the equilibrium position when no imperfections are presented. If we want the expression to be more precise, we could simply substitute x_0 into the right side of the iteration formula in Eq. 14, and then let u_0 equal to the first iteration solution $x_1 = 4Q \cdot E / [m \Omega^2 (a_x(x_0, 0, 0) + q_x^2(x_0, 0, 0)/2)]$, which gives

$$T_{\text{eMM}} \approx \frac{m \Omega^2}{16 k_B} \left(\Delta q + \frac{(x_1 - \delta x)^2}{x_b^2} \right)^2 x_1^2.$$

Appendix C: Numerical Simulation of Ion-Atom Collisions in three Dimensions

In this section a numerical simulation method used for calculating the classical low-energy three-dimensional

ion-atom collision trajectory is introduced. We simulated and compared two situations: the collision happens in a normal Paul trap and the hybrid trap we proposed, respectively. In the following content, we introduce how to calculate the collision process that happened in the hybrid trap, and the situation that happened in the Paul trap can be similarly and easily deduced.

An ^{87}Rb atom of mass m_a approaches an $^{172}\text{Yb}^+$ ion of mass m_i (initially resting in the center of the hybrid trap) from an arbitrary position (in the following content, we take the initial position as $x = 100$ nm, $y = 100$ nm, $z = 100$ nm without loss of generality), by the attractive force between the two, the potential of which originates from the interaction between the ion and polarized atom and thus has the form $-C_4/r^4$, where C_4 represent the polarizability of atom and the value of C_4 is taken from Ref. [14]. For our selected ^{87}Rb - $^{172}\text{Yb}^+$ pair, $C_4 = 160E_h a_0^4$, where E_h is the Hartree energy and a_0 is the Bohr radius. At short ranges, we add a repulsive r^{-6} term to simulate a hard-core potential, where

the hard-core collision distance is on the order of nm when the coefficient C_6 is given as a fraction of C_4 as $C_6 = (10a_0)^2 \times C_4$ in our simulation. Therefore, the total ion-atom potential reads

$$V(r) = -C_4/r^4 + C_6/r^6.$$

Since we intentionally select the magic wavelength $\lambda = 422.3$ nm of the ^{87}Rb atom as the ODT laser wavelength, the only potential experienced by the atom when approaching or moving away is the $V(R)$ above. Thus, the equation of motion of the atom reads

$$m_a \frac{d^2 \mathbf{r}_a}{dt^2} = -\frac{4C_4}{(\mathbf{r}_a - \mathbf{r}_i)^6} (\mathbf{r}_a - \mathbf{r}_i) + \frac{6C_6}{(\mathbf{r}_a - \mathbf{r}_i)^8} (\mathbf{r}_a - \mathbf{r}_i), \quad (\text{C1})$$

where $\mathbf{r}_a = (x_a, y_a, z_a)$ and $\mathbf{r}_i = (x_i, y_i, z_i)$ are the 3D positions of atom and ion separately.

Combining Eq. A16 and the attractive force from the polarized atom, the equation of motion of the ion along the x direction is

$$m_i \frac{d^2 x_i}{dt^2} = -\frac{m_i \Omega^2}{4} [a_x(r_i) + 2q_x(r_i) \cos(\Omega t + \varphi)] x_i + \frac{4C_4}{(r_a - r_i)^6} (x_a - x_i), \quad (\text{C2})$$

and the equations of motion of the ion along the y and z direction can be written down similarly.

We use the explicit Runge-Kutta method of order eight to solve the equations of motion by combining Eq. A17, Eq. A18, Eq. C1 and Eq. C2. Fig. 4 shows a simulated collision trajectory of an atom-ion pair in x , y and z directions respectively. The lifetime of the bound atom-ion pair produced in the hybrid trap is significantly prolonged due to the low RF heating near the hybrid trap center.

Appendix D: Work Done by RF Field on the Ion

When an ion moves in a Paul trap without any disturbance, the RF field does zero work on the ion for an RF period. However, in a cold hybrid ion-atom system, the polarized atom will exert an attraction force on the ion (by attraction potential $V(r) = -C_4/r^4$) and thus disturb the conserved cycle of energy transfer, and finally, the ion-atom system gains net energy from the RF field, which increases the temperature of the system. Here, we calculate the work done by the RF field on the ion when an atom approaches the ion and the collision happens. Suppose the collision point is at r_c , and the collision happens at $t = 0$. When the attraction force between the ion-atom pair dominates, the distance between the ion and atom follows $r(t) = (18C_4/\mu)^{1/6} |t|^{1/3}$, so the trajectory of the ion becomes $r_i(t) = r_c - \mu r(t)/m_i$, where $\mu = m_i m_a / (m_i + m_a)$ is the reduced mass of the ion-atom

pair. We can write down the work done by the RF field on the ion when the atom is close enough to perturb the motion of ion in the trap

$$W = \int_{-t_1}^{t_1} 2q(r_i) \cdot \frac{m_i \Omega^2}{4} r_i \cos(\Omega t + \phi) \dot{r}_i dt,$$

where integration range $t = -t_1 \sim t_1$ is the time when the perturbation from the atom dominates, and we can take $t_1 \approx 0.8$ for approximation[21]. By substituting Eq. B9 and the trajectory of the ion, we get the work done by the RF field during one collision

$$W = W_1 + W_2,$$

$$W_1 = \frac{1}{3} \mu \Omega^2 R^2 \sin \phi \cdot \Delta q \int_0^{\Omega t_1} (A - B\tau^{1/3}) \cdot \tau^{-2/3} \sin \tau \cdot d\tau,$$

$$W_2 = \frac{1}{3} \mu \Omega^2 R^2 \sin \phi \cdot \frac{R^4}{r_0^2 x_b^2} \int_0^{\Omega t_1} (A - B\tau^{1/3})^3 \cdot \tau^{-2/3} \sin \tau \cdot d\tau,$$

where $A = r_c r_0 / R^2$, $B = \mu r_0^2 / m_i R^2$, $r_0 = \sqrt[6]{18C_4 / \mu \Omega^2}$. W_1 comes from the uncompensated alternating force Δq and W_2 comes from the dependence of q on position. For the first collision, when the atom approaches the ion from infinity, the collision happens at $r_{c,0} = 1.11(m_a/m_i)^{5/6} R \approx 20.8$ nm [21], and the numerical results give the max work heating $W_1/k_B \approx -85.2$ nK, $W_2/k_B \approx 27.8$ nK for $\Delta q = -0.001$ at $\sin \phi = 1$. Here

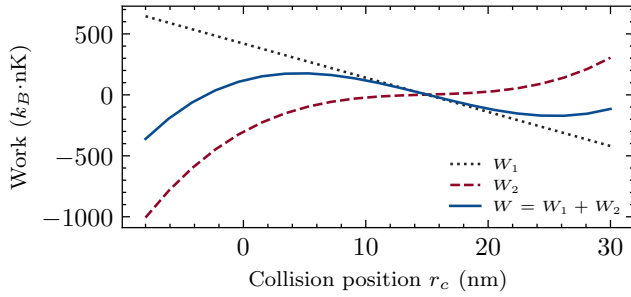


FIG. 5. Maximum work done by the RF field during one collision at $\sin \phi = 1$.

we intentionally choose Δq as negative because we want

$q(r)$ to be nearly 0 at the collision points, not at the origin.

After the first collision happens at $r_{c,0}$, the following collision position $r_{c,i}$ for the i 'th collision is unpredictable. From Fig. 4(a,b) we see that the collisions most likely happen at approximately 0 ~ 20 nm at micromotion directions (x and y axis). The Fig. 5 illustrates the relation of $W = W_1 + W_2$ with r_c for $\Delta q = -0.001$, from which we could see that by compensating the Δq nearly zero, the work done by residual RF field during one collision is on the order of tens of $nK \cdot k_B$. Therefore, the relative energy between an ion-atom pair could easily run below the characteristic energy scale E_k after one or more collisions, making the formation of a bound state (like a molecular ion) possible.

-
- [1] B. R. Heazlewood and T. P. Softley, Towards chemistry at absolute zero, *Nature Reviews Chemistry* **5**, 125 (2021).
 - [2] X. He, K. Wang, J. Zhuang, P. Xu, X. Gao, R. Guo, C. Sheng, M. Liu, J. Wang, J. Li, G. V. Shlyapnikov, and M. Zhan, Coherently forming a single molecule in an optical trap, *Science* **370**, 331 (2020).
 - [3] M.-G. Hu, Y. Liu, D. D. Grimes, Y.-W. Lin, A. H. Gheorghe, R. Vexiau, N. Bouloufa-Maafa, O. Dulieu, T. Rosenband, and K.-K. Ni, Direct observation of bimolecular reactions of ultracold KRb molecules, *Science* **366**, 1111 (2019).
 - [4] J. T. Zhang, Y. Yu, W. B. Cairncross, K. Wang, L. R. B. Picard, J. D. Hood, Y.-W. Lin, J. M. Hutson, and K.-K. Ni, Forming a single molecule by magnetoassociation in an optical tweezer, *Phys. Rev. Lett.* **124**, 253401 (2020).
 - [5] J. D. Hood, Y. Yu, Y. W. Lin, J. T. Zhang, K. Wang, L. R. Liu, B. Gao, and K. K. Ni, Multichannel interactions of two atoms in an optical tweezer, *Phys. Rev. Research* **2**, 023108 (2020).
 - [6] Y. Liu and K.-K. Ni, Bimolecular chemistry in the ultracold regime, *Annu. Rev. Phys. Chem.* **73**, 73 (2022).
 - [7] H. Yang, X.-Y. Wang, Z. Su, J. Cao, D.-C. Zhang, J. Rui, B. Zhao, C.-L. Bai, and J.-W. Pan, Evidence for the association of triatomic molecules in ultracold $23\text{Na}40\text{k} + 40\text{k}$ mixtures, *Nature* **602**, 229 (2022).
 - [8] Z. Su, H. Yang, J. Cao, X.-Y. Wang, J. Rui, B. Zhao, and J.-W. Pan, Resonant control of elastic collisions between $23\text{Na}40\text{k}$ molecules and 40k atoms, *Phys. Rev. Lett.* **129**, 033401 (2022).
 - [9] J. Cao, H. Yang, Z. Su, X.-Y. Wang, J. Rui, B. Zhao, and J.-W. Pan, Preparation of a quantum degenerate mixture of $23\text{Na}40\text{k}$ molecules and 40k atoms, *Phys. Rev. A* **107**, 013307 (2023).
 - [10] L. W. Cheuk, L. Anderegg, Y. Bao, S. Burchesky, S. S. Yu, W. Ketterle, K.-K. Ni, and J. M. Doyle, Observation of collisions between two ultracold ground-state calcium molecules, *Phys. Rev. Lett.* **125**, 043401 (2020).
 - [11] Y. Xie, H. Zhao, Y. Wang, Y. Huang, T. Wang, X. Xu, C. Xiao, Z. Sun, D. H. Zhang, and X. Yang, Quantum interference in $\text{H} + \text{HD} \rightarrow \text{H}_2 + \text{D}$ between direct abstraction and roaming insertion pathways, *Science* **368**, 767 (2020).
 - [12] T. de Jongh, M. Besemer, Q. Shuai, T. Karman, A. van der Avoird, G. C. Groenenboom, and S. Y. T. van de Meerakker, Imaging the onset of the resonance regime in low-energy no-he collisions, *Science* **368**, 626 (2020).
 - [13] A. Härter and J. H. Denschlag, Cold atom-ion experiments in hybrid traps, *Contemp. Phys.* **55**, 33 (2014).
 - [14] M. Tomza, K. Jachymski, R. Gerritsma, A. Negretti, T. Calarco, Z. Idziaszek, and P. S. Julienne, Cold hybrid ion-atom systems, *Rev. Mod. Phys.* **91**, 035001 (2019).
 - [15] N. Zuber, V. S. V. Anasuri, M. Berngruber, Y.-Q. Zou, F. Meinert, R. Löw, and T. Pfau, Observation of a molecular bond between ions and Rydberg atoms, *Nature* **605**, 453 (2022).
 - [16] Y.-Q. Zou, M. Berngruber, V. S. V. Anasuri, N. Zuber, F. Meinert, R. Löw, and T. Pfau, Observation of vibrational dynamics of orientated Rydberg-atom-ion molecules, *Phys. Rev. Lett.* **130**, 023002 (2023).
 - [17] P. Weckesser, F. Thielemann, D. Wiater, A. Wojciechowska, L. Karpa, K. Jachymski, M. Tomza, T. Walker, and T. Schaetz, Observation of Feshbach resonances between a single ion and ultracold atoms, *Nature* **600**, 429 (2021).
 - [18] H. Hirzler, R. S. Lous, E. Trimby, J. Pérez-Ríos, A. Safavi-Naini, and R. Gerritsma, Observation of Chemical Reactions between a Trapped Ion and Ultracold Feshbach Dimers, *Phys. Rev. Lett.* **128**, 103401 (2022).
 - [19] O. Katz, M. Pinkas, N. Akerman, and R. Ozeri, Quantum logic detection of collisions between single atom-ion pairs, *Nat. Phys.* **18**, 533 (2022).
 - [20] T. Feldker, H. Furst, H. Hirzler, N. V. Ewald, M. Mazzanti, D. Wiater, M. Tomza, and R. Gerritsma, Buffer gas cooling of a trapped ion to the quantum regime, *Nat. Phys.* **16**, 413 (2020).
 - [21] M. Cetina, A. T. Grier, and V. Vuletić, Micromotion-Induced Limit to Atom-Ion Sympathetic Cooling in Paul Traps, *Phys. Rev. Lett.* **109**, 253201 (2012).
 - [22] M. Pinkas, O. Katz, J. Wengrowicz, N. Akerman, and R. Ozeri, Trap-assisted formation of atom-ion bound

- states, *Nature Physics* **19**, 1573 (2023).
- [23] H. Hirzler, E. Trimby, R. Gerritsma, A. Safavi-Naini, and J. Pérez-Ríos, Trap-Assisted Complexes in Cold Atom-Ion Collisions, *Phys. Rev. Lett.* **130**, 143003 (2023).
 - [24] C. Schneider, M. Enderlein, T. Huber, and T. Schaetz, Optical trapping of an ion, *Nat. Photonics* **4**, 772 (2010).
 - [25] T. Huber, A. Lambrecht, J. Schmidt, L. Karpa, and T. Schaetz, A far-off-resonance optical trap for a Ba⁺ ion, *Nat. Commun.* **5**, 5587 (2014).
 - [26] J. Schmidt, A. Lambrecht, P. Weckesser, M. Debatin, L. Karpa, and T. Schaetz, Optical Trapping of Ion Coulomb Crystals, *Phys. Rev. X* **8**, 021028 (2018).
 - [27] J. Schmidt, P. Weckesser, F. Thielemann, T. Schaetz, and L. Karpa, Optical Traps for Sympathetic Cooling of Ions with Ultracold Neutral Atoms, *Phys. Rev. Lett.* **124**, 053402 (2020).
 - [28] T. F. Gloger, P. Kaufmann, D. Kaufmann, M. T. Baig, T. Collath, M. Johanning, and C. Wunderlich, Ion-trajectory analysis for micromotion minimization and the measurement of small forces, *Phys. Rev. A* **92**, 043421 (2015).
 - [29] R. Grimm, M. Weidemüller, and Y. B. Ovchinnikov, Optical Dipole Traps for Neutral Atoms, in *Advances In Atomic, Molecular, and Optical Physics*, Vol. 42, edited by B. Bederson and H. Walther (Elsevier, 2000) pp. 95–170.
 - [30] D. J. Berkeland, J. D. Miller, J. C. Bergquist, W. M. Itano, and D. J. Wineland, Minimization of ion micromotion in a Paul trap, *J. Appl. Phys.* **83**, 5025 (1998).
 - [31] M. Drewsen and A. Brøner, Harmonic linear Paul trap: Stability diagram and effective potentials, *Phys. Rev. A* **62**, 045401 (2000).
 - [32] Z.-H. Qian, J.-M. Cui, X.-W. Luo, Y.-X. Zheng, Y.-F. Huang, M.-Z. Ai, R. He, C.-F. Li, and G.-C. Guo, Super-resolved Imaging of a Single Cold Atom on a Nanosecond Timescale, *Phys. Rev. Lett.* **127**, 263603 (2021).
 - [33] V. Blums, M. Piotrowski, M. I. Hussain, B. G. Norton, S. C. Connell, S. Gensemer, M. Lobino, and E. W. Streed, A single-atom 3D sub-attoneutron force sensor, *Sci. Adv.* **4**, eaao4453 (2018).
 - [34] J. D. Wong-Campos, K. G. Johnson, B. Neyenhuis, J. Mizrahi, and C. Monroe, High-resolution adaptive imaging of a single atom, *Nat. Photonics* **10**, 606 (2016).
 - [35] R. He, J.-M. Cui, R.-R. Li, Z.-H. Qian, Y. Chen, M.-Z. Ai, Y.-F. Huang, C.-F. Li, and G.-C. Guo, An ion trap apparatus with high optical access in multiple directions, *Rev. Sci. Instrum.* **92**, 073201 (2021).
 - [36] Website of the data availability, <https://zenodo.org/records/15179965> (2025), accessed: 2025-04-06.